Crimsonite, $PbFe_2^{3+}(PO_4)_2(OH)_2$, the phosphate analogue of carminite from the Silver Coin mine, Valmy, Nevada, USA

A. R. Kampf[1,*], P. M. Adams[2], S. J. Mills[3] and B. P. Nash[4]

[1] Mineral Sciences Department, Natural History Museum of Los Angeles County, 900 Exposition Boulevard, Los Angeles, CA 90007, USA
[2] 126 South Helberta Avenue #2, Redondo Beach, California 90277, USA
[3] Geosciences, Museum Victoria, GPO Box 666, Melbourne 3001, Victoria, Australia
[4] Department of Geology and Geophysics, University of Utah, Salt Lake City, UT 84112, USA

ABSTRACT

Crimsonite (IMA2014-095), $PbFe_2^{3+}(PO_4)_2(OH)_2$, the phosphate analogue of carminite, is a new mineral from the Silver Coin mine, Valmy, Iron Point district, Humboldt County, Nevada, USA, where it occurs as a low-temperature secondary mineral in association with fluorwavellite, goethite, hematite, hentschelite, plumbogummite and variscite on quartz. Crimsonite occurs in subparallel aggregates of deep red blades or plates flattened on {100} and up to 0.1 mm in maximum dimension. The streak is light purplish orange. Crystals are transparent and have adamantine lustre. The Mohs hardness is ∼3½, the tenacity is brittle, the fracture is irregular to splintery and an imperfect cleavage is likely on {101}. The calculated density is 5.180 g/cm³. Crimsonite is optically biaxial (+), with $2V = 85.5(5)°$ and $\gamma - \alpha = 0.011$. Using the Gladstone-Dale relationship, the calculated indices of refraction are $\alpha = 2.021$, $\beta = 2.026$ and $\gamma = 2.032$. The optical orientation is $X = \mathbf{b}$; $Y = \mathbf{a}$; $Z = \mathbf{c}$ and the pleochroism is X light orange, Y light yellow, Z red brown; $Y < X < Z$. Electron microprobe analyses provided PbO 40.69, CaO 0.60, ZnO 0.72, CuO 0.13, Fe_2O_3 23.36, Al_2O_3 0.34, V_2O_5 0.70, As_2O_5 12.05, P_2O_5 16.03, SO_3 0.33 and H_2O 3.64 (structure), total 98.59 wt.%. The empirical formula (based on 10 O apfu) is $(Pb_{1.06}Ca_{0.06})_{\Sigma1.12}(Fe_{1.71}Zn_{0.05}Al_{0.04}Cu_{0.01})_{\Sigma1.81}(P_{1.32}As_{0.61}V_{0.05}S_{0.02})_{\Sigma2.00}O_8[(OH)_{1.64}(H_2O)_{0.36}]_{\Sigma2.00}$. Crimsonite is orthorhombic, *Cccm*, $a = 16.2535(13)$, $b = 7.4724(4)$, $c = 12.1533(9)$ Å, $V = 1476.04(17)$ Å³ and $Z = 8$. The eight strongest lines in the powder X-ray diffraction pattern are [d_{obs} in Å$(I)(hkl)$]: 5.86(42)(111); 4.53(45)(112); 3.485(64)(113); 3.190(100)(022); 3.026(40)(004); 2.902(54)(511); 2.502(77)(422) and 2.268(54)(224). The structure of crimsonite ($R_1 = 3.57\%$ for 740 $F_o > 4\sigma F$) contains FeO_6 octahedra that share edges to form dimers, which are then linked to other dimers by corner sharing to form chains along [010]. These chains are linked by PO_4 tetrahedra yielding sheets parallel to {001}. The sheets are linked to one another via bonds to 8-coordinated Pb^{2+} atoms with non-stereoactive $6s^2$ lone-electron pairs.

Introduction

The Silver Coin mine, a small base-metal deposit in north-central Nevada (USA), was last worked, principally for silver, in 1929. Since the late 1980s, the mine has been a popular site for collectors in search of rare mineral species. To date, seven new mineral species have been described from here: zinclipscombite (Chukanov *et al.*, 2006), meurigite-Na (Kampf *et al.*, 2009), iangreyite (Mills *et al.*, 2011), krásnoite (Mills *et al.*, 2012), fluorowardite (Kampf *et al.*, 2014), ferribushmakinite (Kampf *et al.*, 2015*b*) and fluorwavellite (Kampf *et al.*, 2015*c*).

Herein, we describe crimsonite, the seventh new mineral species from this mine. The name is

based upon the mineral's deep red (crimson) colour and the fact that it is the phosphate analogue of carminite, a mineral with a very similar deep red colour and whose name is also based upon its colour (carmine). The new mineral and name have been approved by the Commission on New Minerals, Nomenclature and Classification of the International Mineralogical Association (IMA2014-095, Kampf *et al.*, 2015*a*). The holotype specimen is housed in the collections of the Mineral Sciences Department, Natural History Museum of Los Angeles County, catalogue number 65558.

Occurrence and paragenesis

Crimsonite occurs on a single small specimen collected from the ceiling of the Phosphate stope at the Silver Coin mine, Valmy, Iron Point district, Humboldt County, Nevada, USA (40°55'44″N, 117°19'26″W). The mineral is a low-temperature secondary mineral associated with fluorwavellite,

goethite, hematite, hentschelite, plumbogummite and variscite on quartz. We have now confirmed more than 130 mineral species from the Silver Coin mine. The vast majority of these are from the Phosphate stope. A partial list was provided by Thomssen and Wise (2004) and updates were provided by Kampf *et al.* (2009, 2014, 2015) and Mills *et al.* (2011, 2012). Adams *et al.* (2015) provide a complete, up-to-date description of the Silver Coin mine and its mineralogy.

At the Silver Coin mine, quartz veins containing argentiferous galena, sphalerite and pyrite were emplaced, in part, along faults and fractures in phosphatic argillites. When exposed to vadose water, the pyrite and other sulfides were oxidized, producing acidic fluids that leached PO_4 and Al from the argillite wall rocks. The prolific secondary assemblage then precipitated along fractures and bedding planes.

Physical and optical properties

Crimsonite occurs in subparallel aggregates of blades or plates up to 0.1 mm in maximum dimension (Figs 1 and 2). The blades are flattened on {100}, somewhat elongated on [010] and exhibit the forms {100}, {101} and {011} (Fig. 3). No twinning was observed. The colour of the mineral is deep red with a slight purplish cast and it has a light purplish-orange streak. Crystals are transparent and have adamantine lustre. Crimsonite does not fluoresce in longwave or shortwave ultraviolet light. The Mohs hardness is probably ~3½ by analogy with carminite, the tenacity is brittle and the fracture is irregular. No cleavage was observed,

FIG. 1. Crimsonite crystals growing on plumbogummite that, in turn, is coating quartz. The field of view is 0.4 mm across. NHMLAC specimen number 65558.
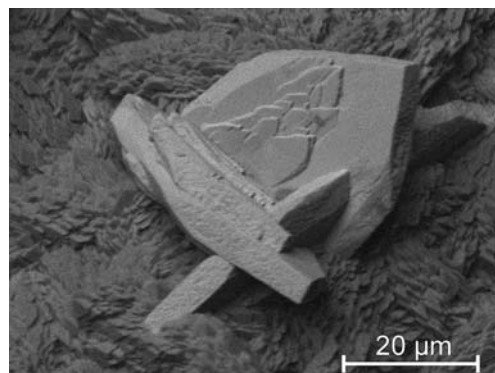

FIG. 2. Electron back-scatter scanning electron micrscope image of crimsonite crystals on plumbogummite. NHMLAC specimen number 65558.
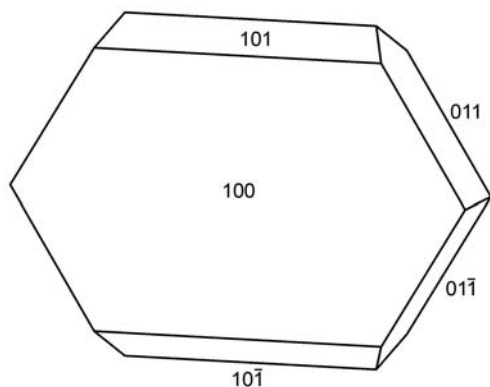
FIG. 3. Crystal drawing of crimsonite (clinographic projection).

but an imperfect cleavage on {101} is likely by analogy with carminite (based on the modern cell setting with $a > c > b$). The density could not be measured because it is greater than those of available high-density liquids and there is insufficient material for physical measurement. The calculated density based on the empirical formula and the unit cell refined from the single-crystal data is 5.180 g/cm^3. Crimsonite is insoluble at room temperature in concentrated HCl and 70% HNO$_3$.

Crimsonite is optically biaxial (+). The 2V determined from extinction data using *EXCALIBR* (Gunter *et al.*, 2004) is 85.5(5)°. The birefringence $\gamma - \alpha = 0.011$ was measured with a Berek compensator. The indices of refraction could not be measured because they are higher than available index liquids; however, using the average index of refraction of 2.026 predicted by the Gladstone-Dale relationship (Mandarino, 1981), along with the measured 2V and $\gamma - \alpha$ birefringence, the indices of refraction can be calculated to be $\alpha = 2.021$, $\beta = 2.026$ and $\gamma = 2.032$. The optical orientation is $X = \mathbf{b}$; $Y = \mathbf{a}$; $Z = \mathbf{c}$ and the pleochroism is X light orange, Y light yellow, Z red brown; $Y < X < Z$. The dispersion could not be observed.

Chemical composition

Quantitative analyses (22 points on nine crystals from a single small specimen) were performed at the University of Utah using a Cameca SX-50 electron microprobe with four wavelength-dispersive spectrometers utilizing *Probe* for electron probe microanalysis (EPMA) software. Analytical conditions were 15 kV accelerating voltage, 20 nA beam current and a beam diameter of 5–10 μm. The sample showed no visible damage under the electron beam. Raw X-ray intensities were corrected for matrix effects with a $\phi(\rho z)$ (PAP) algorithm (Pouchou and Pichoir, 1991).

The contents of P and As exhibited a strong negative correlation, from $P/(P + As) = 0.52$ to 0.79, but the variation appears to be unrelated to growth zonation, i.e. no core-to-rim variation in composition was observed. The minor contents of V and S in the tetrahedral P site also varied, with V increasing and S decreasing with P content.

There was insufficient material for CHN analyses, so H$_2$O was calculated on the basis of P + As + V + S = 2, charge balance and 10 O atoms per formula unit (apfu), as determined by the crystal structure analysis (see below). The tiny crystals do not take a good polish, which contributes to the low analytical total. Analytical data are given in Table 1. No other elements were detected by energy-dispersive spectroscopy. Other probable elements were sought by wavelength-dispersive spectroscopy EPMA.

The empirical formula (based on 10 O apfu) is $(Pb_{1.06}Ca_{0.06})_{\Sigma1.12}(Fe_{1.71}Zn_{0.05}Al_{0.04}Cu_{0.01})_{\Sigma1.81}$ $(P_{1.32}As_{0.61}V_{0.05}S_{0.02})_{\Sigma2.00}O_8[(OH)_{1.64}(H_2O)_{0.36}]_{\Sigma2.00}$. The ideal formula is $PbFe_2^{3+}(PO_4)_2(OH)_2$, which requires PbO 41.12, Fe$_2$O$_3$ 29.42, P$_2$O$_5$ 26.15 and H$_2$O 3.32, total 100 wt.%. The structure refinement (see below) shows an extra low-occupancy large-cation site near the less-than-fully-occupied octahedral-cation site. This provides a structural basis for the significant large-cation excess and the significant octahedral-cation deficiency observed in the empirical formula.

X-ray crystallography and structure refinement

Both powder and single-crystal X-ray studies were carried-out using a Rigaku R-Axis Rapid II curved imaging plate microdiffractometer, with monochromatized Mo$K\alpha$ radiation. For the powder-diffraction study, a Gandolfi-like motion on the φ and ω axes was used to randomize the sample and observed d spacings and intensities were derived by profile fitting using *JADE 2010* software (Materials Data, Inc., USA). The observed powder data are presented in Table 2, along with the d values and intensities calculated from the structure, also using *JADE 2010*. Unit-cell parameters refined from the powder data using *JADE 2010* with whole pattern fitting are: $a = 16.2573(16)$, $b = 7.4692(7)$, $c = 12.1406(12)$ Å and $V = 1474.2(2)$ Å^3.

TABLE 1. Electron microprobe data for crimsonite.

Constituent	Wt.%	min	max	SD	Probe standard
PbO	40.69	37.56	44.56	1.61	Pb metal
CaO	0.60	0.21	0.83	0.18	diopside
ZnO	0.72	0.51	1.01	0.12	ZnO (syn)
CuO	0.13	0.00	0.27	0.07	Cu metal
Fe_2O_3	23.36	20.29	25.37	1.06	hematite
Al_2O_3	0.34	0.22	0.76	0.11	YAG
V_2O_5	0.70	0.21	1.20	0.27	Y vanadate (syn)
As_2O_5	12.05	8.31	17.03	2.37	GaAs (syn)
P_2O_5	16.03	11.56	19.09	2.00	apatite
SO_3	0.33	0.17	0.65	0.11	celestine
H_2O*	3.64				
Total	98.59				

* Based on the structure
SD – standard deviation

The Rigaku *CrystalClear* software package was used for processing of structure data, including the application of an empirical multi-scan absorption correction using *ABSCOR* (Higashi, 2001). *SHELXL-97* software (Sheldrick, 2008) was used for the refinement of the structure. The starting atom coordinates for the structure refinement were taken from the structure determination of carminite by Kharisun *et al.* (1996). The small size of crimsonite crystals and their occurrence in subparallel intergrowths made the selection of a crystal for structure work very challenging. The small size (40 µm × 30 µm × 10 µm) and less than optimal quality of the crystal fragment used might account for some anomalies in the results of the structure refinement. Details of the data collection and structure refinement are provided in Table 3. Fractional coordinates and atom displacement parameters are provided in Table 4, selected interatomic distances in Table 5 and bond valences in Table 6.

The Pb1 and Pb2 sites were assigned occupancy only by Pb, the Fe site was assigned occupancy only by Fe and the P1 and P2 sites were assigned joint occupancy by P and As. In the final refinement, the occupancies of all of these sites were refined. Both Pb sites and the Fe sites refined to significantly less than full occupancy. Some of the occupancy deficiencies can be accounted for by partial Ca occupancy in the Pb sites and partial Al occupancy in the Fe site, but the small amounts of these constituents indicated by the chemical analyses are insufficient to completely account for the low scattering powers of the sites.

The P1 and P2 sites, assigned full occupancy by P + As, refined to $P_{0.62}As_{0.38}$ and $P_{0.95}As_{0.05}$, respectively, indicating a preference of As for the P1 site and a preference of P for the P2 site. These preferences are consistent with the P–O bond distances, which are significantly shorter for the P2 site. For the higher As compositions mentioned above that are close to the midpoint in the series between carminite and crimsonite (i.e. P/(P + As) = 0.52), it seems likely that the P1 site is dominantly As, while the P2 is dominantly P. A structure refinement on such material, definitively demonstrating separate As- and P-dominant sites, would presumably qualify it as a distinct ordered-intermediate species.

A large electron density residual ($\sim$4e) located 1.13 Å from the Fe site appears to represent a third Pb site (Pb3) with very low occupancy (0.024). This Pb would locally replace the Fe and O7 sites and would have a coordination consistent with it having a stereoactive $6s^2$ lone-electron pair (Table 5; Fig. 4). As noted above, this provides a possible explanation for the significant large-cation excess and the significant octahedral-cation deficiency observed in the empirical formula, but only if the Pb1 and Pb2 sites are assumed to contain more Pb than the refinement indicates.

Discussion

Crimsonite is isostructural with carminite, $PbFe_2^{3+}(AsO_4)_2(OH)_2$ and sewardite, $CaFe_2^{3+}(AsO_4)_2(OH)_2$ (Roberts *et al.*, 2002). In the

TABLE 2. Powder X-ray diffraction data for crimsonite.

I_{obs}	d_{obs}	d_{calc}	I_{calc}	hkl	I_{obs}	d_{obs}	d_{calc}	I_{calc}	hkl
		8.1268	3	2 0 0			1.7911	8	7 1 4
10	6.84	6.7893	5	1 1 0	39	1.7806	1.7807	12	0 2 6
42	5.86	5.9271	25	1 1 1			1.7783	12	6 2 4
26	4.88	4.8666	20	2 0 2			1.7768	17	5 3 3
45	4.53	4.5279	46	1 1 2			1.7440	5	2 4 2
24	4.39	4.3862	32	3 1 0			1.7125	6	8 2 2
35	4.12	4.1258	26	3 1 1			1.6984	3	7 3 0
		4.0634	10	4 0 0	30	1.6966	1.6973	28	4 4 0
14	3.569	3.5565	15	3 1 2			1.6864	3	9 1 2
64	3.485	3.4789	63	1 1 3			1.6821	3	7 3 1
		3.3946	5	2 2 0			1.6754	6	5 1 6
		3.2695	14	2 2 1	18	1.6598	1.6572	18	5 3 4
100	3.190	3.1827	100	0 2 2			1.6563	2	3 3 5
40	3.026	3.0383	23	0 0 4			1.6381	2	7 1 5
35	2.983	2.9809	38	5 1 0	18	1.6258	1.6310	12	4 2 6
		2.9760	2	3 1 3			1.6222	8	6 0 6
54	2.902	2.8950	57	5 1 1			1.6143	2	3 1 7
29	2.777	2.7733	33	1 1 4			1.6107	9	9 1 3
27	2.679	2.6762	35	5 1 2	12	1.5926	1.5914	17	0 4 4
11	2.604	2.6019	11	2 2 3			1.5702	7	10 0 2
77	2.502	2.5056	74	4 2 2			1.5457	3	2 2 7
		2.4742	19	6 0 2			1.5338	9	5 3 5
		2.4621	8	1 3 0	22	1.5203	1.5200	9	9 1 4
36	2.429	2.4333	23	4 0 4			1.5192	14	0 0 8
		2.4130	10	1 3 1			1.5093	2	3 3 6
		2.4009	11	5 1 3			1.5003	9	5 1 7
		2.2884	12	1 1 5			1.4955	2	7 1 6
		2.2819	5	1 3 2	19	1.4916	1.4904	13	10 2 0
54	2.268	2.2639	36	2 2 4			1.4882	2	1 5 0
6	2.220	2.2248	2	3 3 1			1.4772	4	1 5 1
		2.2173	2	7 1 0			1.4621	3	9 3 0
		2.1813	2	7 1 1			1.4516	4	9 3 1
		2.1583	6	6 2 1			1.4495	2	11 1 0
14	2.131	2.1278	10	5 1 4			1.4455	3	1 5 2
		2.1208	5	3 3 2			1.4393	3	11 1 1
		2.0830	5	7 1 2			1.4355	2	3 1 8
10	2.034	2.0317	14	8 0 0	10	1.4223	1.4231	6	9 1 5
		1.9771	4	5 3 0			1.4215	5	9 3 2
13	1.9716	1.9757	8	3 3 3			1.4189	2	1 3 7
		1.9654	6	2 0 6			1.4148	5	5 3 6
21	1.9448	1.9515	7	5 3 1			1.3866	2	2 2 8
		1.9451	6	7 1 3			1.3753	2	9 3 3
		1.9410	9	1 1 6			1.3613	2	6 2 7
		1.9286	3	6 2 3	8	1.3518	1.3540	4	2 4 6
18	1.8822	1.8838	11	5 1 5			1.3535	5	5 1 8
		1.8801	7	5 3 2			1.3495	2	5 5 1
		1.8681	7	0 4 0	8	1.3351	1.3381	16	10 2 4
8	1.812	1.8150	12	3 3 4			1.3266	3	9 1 6

Note: Calculated lines with intensities < 2 are not shown.

TABLE 3. Data collection and structure refinement details for crimsonite.*

Diffractometer	Rigaku R-Axis Rapid II
X-ray radiation / power	$MoK\alpha$ ($\lambda = 0.71075$ Å) / 50 kV, 40 mA
Temperature	298(2) K
Structural formula	$Pb_{0.90}Fe_{1.68}(P_{1.57}As_{0.43})_{\Sigma2.00}O_8(OH)_2$
Space group	*Cccm*
Unit-cell dimensions	$a = 16.2535(13)$ Å
	$b = 7.4724(4)$ Å
	$c = 12.1533(9)$ Å
V	1476.04(17) Å^3
Z	8
Density (for above formula)	4.713 g/cm^3
Absorption coefficient	26.114 mm^{-1}
F(000)	1899.4
Crystal size (μm)	$40 \times 30 \times 10$
θ range (°)	3.00 to 27.48
Frames/width/time	27/5°/45 min
Index ranges	$-20 \le h \le 20$, $-7 \le k \le 9$, $-14 \le l \le 15$
Reflections collected / unique	4212/881 [$R_{int} = 0.046$]
Reflections with $F_o > 4\sigma(F)$	740
Completeness to $\theta = 27.48°$	99.2%
Max. and min. transmission	0.421 and 0.780
Refinement method	Full-matrix least-squares on F^2
Parameters refined	82
Goof	1.140
Final *R* indices [$F_o > 4\sigma(F)$]	$R_1 = 0.0357$, w$R_2 = 0.0685$
R indices (all data)	$R_1 = 0.0466$, w$R_2 = 0.0725$
Largest diff. peak / hole	$+1.495$ / -1.008 e/A^3

*$R_{int} = \Sigma|F_o^2 - F_o^2$ (mean)$|/\Sigma[F_o^2]$. Goof $= S = \{\Sigma[w(F_o^2 - F_c^2)^2]/(n-p)\}^{1/2}$.
$R_1 = \Sigma||F_o|-|F_c||/\Sigma|F_o|$. $wR_2 = \{\Sigma[w(F_o^2 - F_c^2)^2]/\Sigma[w(F_o^2)^2]\}^{1/2}$. $w = 1/[\sigma^2(F_o^2)$
$+ (aP)^2 + bP]$ where a is 0.0185, b is 42.8723 and P is $[2F_c^2 + Max(F_o^2,0)]/3$.

crimsonite structure (Fig. 5), FeO$_6$ octahedra share edges to form dimers which are then linked to other dimers by corner sharing to form chains along [010]. These chains are linked by PO$_4$ tetrahedra yielding sheets parallel to {001}. The sheets are linked to one another via bonds to 8-coordinate Pb^{2+} atoms. The Pb1 and Pb2 sites are on centres of symmetry and thus the lone-electron pairs of these Pb^{2+} atoms are not stereoactive.

Bond-valence sums (BVS) for the O atoms in the crimsonite structure are similar to those for the structures of carminite and sewardite. The hydrogen bonding clearly involves O3, O6 and O7 based upon bond distances and BVS. The O6 and O7 atoms are probably OH groups; however, the BVS of O6 (1.00 valence units, vu) is less than normal for an OH group and the BVS of O7 (1.52 vu) is greater than normal for an OH group. As noted by Kharisun *et al.* (1996) for carminite, the O7–O7 distance (2.58 Å for carminite and 2.59 Å for crimsonite) is consistent with one H atom between the two O7 atoms. This H is assumed to be disordered over two sites (e.g. corresponding to O7–H = 0.9 Å and H···O7 = 1.69 Å) and the ½ H per O7 yields a BVS of $1.52 + 0.50 = 2.02$ vu. The O6 atom can form hydrogen bonds to O3 (at 2.76 Å) and another O6 (at 2.66 Å). The BVS suggests that O6 has some H$_2$O character. Assuming it to be ½ OH and ½ H$_2$O and that it forms one full hydrogen bond to O3 and ½ hydrogen bond to O6, the BVS of O3 is $1.56 + 0.20 = 1.76$ vu and that for O6 is $1.00 + 0.25 + 0.80 = 2.05$ vu. It is also worth noting that a vacancy at the Fe site is probably coupled to H$_2$O presence at the O6 site. For purposes of establishing an ideal formula, it seems preferable to consider O6 and O7 as both being predominantly OH, as the describers of carminite and sewardite have done. This yields $PbFe_2^{3+}(PO_4)_2(OH)_2$.

The BVS results for the cations are somewhat in variance with the structural and empirical formulae.

TABLE 4. Atom coordinates and displacement parameters (Å^2) for crimsonite.

	Occ.	x/a	y/b	z/c	U_{eq}	U^{11}	U^{22}	U^{33}	U^{23}	U^{13}	U^{12}
Pb1	0.912(9)	0	0	0.25	0.0194(2)	0.0210(4)	0.0162(4)	0.0209(4)	0	0	0
Pb2	0.799(9)	0.25	0.75	0	0.0166(3)	0.0192(4)	0.0146(4)	0.0159(4)	0	0	−0.0011(3)
Pb3	0.0236(17)	0.3970(9)	0.0439(19)	0.2054(14)	0.024(5)						
Fe	0.840(10)	0.37520(9)	0.13145(16)	0.13506(10)	0.0103(4)	0.0111(7)	0.0109(7)	0.0090(6)	−0.0002(5)	0.0006(5)	−0.0024(5)
P1	0.622(13)	0.04370(11)	0.7391(2)	0	0.0089(6)	0.0109(9)	0.0075(9)	0.0082(9)	0	0	0.0004(6)
As1	0.378(13)										
P2	0.947(10)	0.21048(14)	0	0.25	0.0052(8)	0.0058(13)	0.0053(12)	0.0044(12)	0.0007(9)	0	0
As2	0.053(10)										
O1	1	0.0152(4)	0.2503(7)	0.1074(5)	0.0178(13)	0.019(3)	0.019(3)	0.015(3)	0.000(2)	0.000(2)	−0.006(2)
O2	1	0.0957(5)	0.5496(11)	0	0.020(2)	0.025(5)	0.022(4)	0.013(4)	0	0	0.005(3)
O3	1	0.1100(6)	−0.1035(13)	0	0.033(2)	0.046(7)	0.026(5)	0.026(5)	0	0	−0.005(4)
O4	1	0.1532(3)	0.1676(8)	0.2406(5)	0.0196(14)	0.017(3)	0.019(3)	0.023(3)	0.002(3)	0.001(3)	0.002(2)
O5	1	0.2666(3)	−0.0062(8)	0.1456(4)	0.0180(13)	0.014(3)	0.027(3)	0.013(2)	−0.004(3)	0.001(2)	−0.002(2)
O6	1	0.1682(5)	0.2427(9)	0	0.0104(16)						
O7	1	0.4203(5)	0	0.25	0.0157(18)						

TABLE 5. Selected bond distances (Å) in crimsonite.

Pb1–O1(× 4)	2.562(5)	Pb2–O3(×2)	2.525(10)	Pb3–O5	2.271(15)	Fe–O7	1.859(4)	Hydrogen bonds
Pb1–O4(×4)	2.790(6)	Pb2–O5(×4)	2.554(6)	Pb3–O4	2.345(15)	Fe–O1	2.016(6)	O6–O3 2.755(12)
<Pb1–O>	2.676	Pb2–O2(×2)	2.921(8)	Pb3–O1	2.412(16)	Fe–O6	2.019(4)	O6–O6 2.660(15)
		<Pb2–O>	2.639	Pb3–O2	2.595(16)	Fe–O4	2.028(6)	O7–O7 2.590(18)
				Pb3–O5	2.801(16)	Fe–O5	2.047(6)	
P1–O3	1.595(10)			Pb3–O4	3.000(16)	Fe–O2	2.179(5)	
P1–O1(×2)	1.621(6)	P2–O5(×2)	1.563(5)	Pb3–O7	3.036(18)	<Fe–O>	1.993	
P1–O2	1.649(8)	P2–O4(×2)	1.565(6)	Pb3–O1	3.150(17)			
<P1–O>	1.622	<P2–O>	1.564	Pb3–O1	3.351(16)			
				Pb3–O1	3.467(17)			
				Pb3–O2	3.582(17)			

TABLE 6. Bond-valence analysis for crimsonite.*
Values are expressed in valence units.

	O1	O2	O3	O4	O5	O6	O7	Σ
Pb1	0.29 ×4→			0.18 ×4→				1.88
Pb2		0.14 ×2→	0.32 ×2→		0.30 ×4→			2.12
Fe	0.50	0.32 ×2↓		0.48	0.46	0.50 ×2↓	0.76 ×2↓	3.02
P1	1.15 ×2→	1.07	1.24					4.61
P2				1.14 ×2→	1.15 ×2→			4.58
Σ	1.94	1.85	1.56	1.80	1.91	1.00	1.52	

*The bond strengths are based upon full occupancies, Pb1 and Pb2 sites only by Pb, Fe site only by Fe and P1 and P2 sites by P + As. Multiplicity is indicated by ×↓→. Fe^{3+}–O and As^{5+}–O bond-valence parameters are from Brown and Altermatt (1985), P^{5+}–O are from Brese and O'Keeffe (1991) and Pb^{2+}–O are from Krivovichev and Brown (2001). Hydrogen-bond contributions are not included.

The bond-valence sums for the Pb sites are consistent with close to full occupancy, in agreement with the empirical formula, but not the refined occupancies. The BVS for the Fe site (neglecting minor constituents) suggests full occupancy by Fe, while both the chemical analysis and structure refinement indicate less than stoichiometric Fe. Most notably, the bond-valence sums for the P1 and P2 sites (4.61 and 4.58 vu), based on the refined P/As occupancies, are much lower than optimal (5) for these occupancies. These bond-valence sums were computed using the bond-valence parameter for the P^{5+}–O bond recommended by Brese and O'Keeffe (1991), 1.604, and that for the As^{5+}–O bond recommended by Brown and Altermatt (1985), 1.767. If the bond-valence parameter for P^{5+}–O recommended by Brown and Altermatt (1985), 1.617, is used instead of 1.604, the situation is improved, but the bond-valence sums are still significantly low (4.70 and 4.74 vu).

Carminite, while not a common mineral, is far more common than crimsonite. Carminite has been reported from nearly 200 localities worldwide (see www.mindat.org). One factor that might help to explain the more common occurrence of carminite is that Pb^{2+} and Fe^{3+} more commonly occur in geological environments (mainly oxidation zones of base-metal deposits) with AsO_4^{3-} than they do in those with PO_4^{3-}, but this clearly does not tell the whole story. The low bond-valence sums for the P1 and P2 sites in the crimsonite structure suggest that
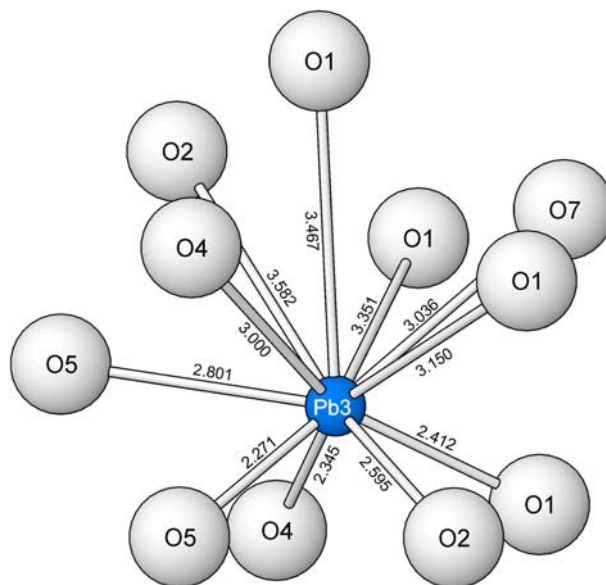

FIG. 4. The coordination of the low-occupancy Pb3 site. The O7, Fe, Pb3 and Fe sites at 0.738, 1.134, 1.266 and 2.366 Å, respectively, from Pb3 are presumed to be vacant when the Pb3 site is occupied. Note the off-centre position of Pb3, typical of Pb^{2+} with stereoactive lone-pair electrons.
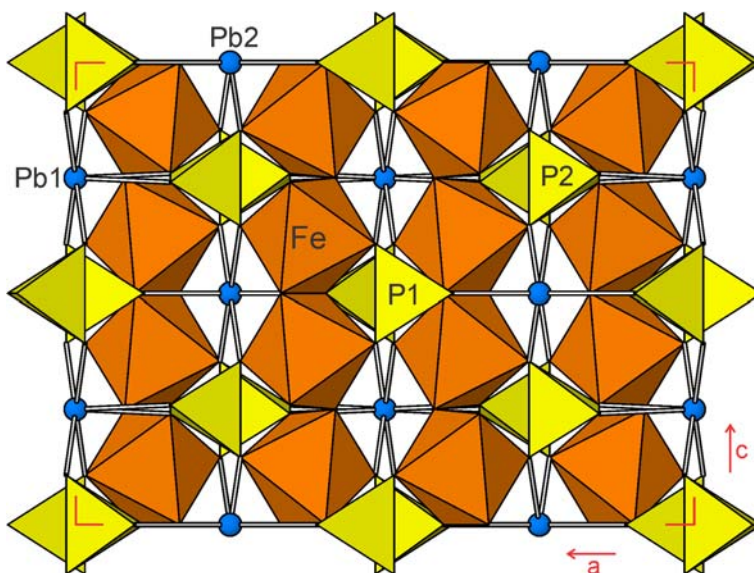
FIG. 5. The structure of crimsonite viewed along [010]. The low-occupancy Pb3 site is not shown.

the structure is not flexible enough to allow optimal P–O bond lengths, and suggests that the structure inherently prefers As over P in its tetrahedral sites. This conclusion is also supported by the fact that reported carminite compositions generally are lacking in P, while crimsonite contains a substantial amount of As, even though its association with dominantly PO_4-bearing phases (fluorwavellite, hentschelite, plumbogummite and variscite) indicates a relatively AsO_4-poor environment. It seems clear that crimsonite will only form in environments much richer in PO_4 than AsO_4; in more AsO_4-rich environments carminite will form. However, the structure of crimsonite very likely requires some As^{5+} in its tetrahedral cation sites for stability. Our conclusion is that crimsonite will probably only form in PO_4-rich environments in which a small amount of AsO_4 is also present.

A more difficult question is why the phosphate analogue of carminite formed at all, instead of one of the other known minerals containing essential Pb^{2+}, Fe^{3+} and PO_4^{3-}: corkite, $PbFe_3^{3+}(PO_4)(SO_4)$ $(OH)_6$, drugmanite, $Pb_2Fe^{3+}(PO_4)(PO_3OH)(OH)_2$, ferribushmakinite, $Pb_2Fe^{3+}(PO_4)(VO_4)(OH)$, kintoreite, $PbFe_3^{3+}(PO_4)(PO_3OH)(OH)_6$ and pattersonite, $PbFe_3^{3+}(PO_4)_2(OH)_5 \cdot H_2O$. Of these, corkite, ferribushmakinite and kintoreite have been found at the Silver Coin mine, but not in direct association with crimsonite. Composition, pH and possibly temperature constraints provide the most likely

answers. Although some VO_4 and SO_4 are present in crimsonite, we conjecture that the amounts available in the local environment were insufficient to form ferribushmakinite or corkite, respectively. Drugmanite and kintoreite, both of which contain acid phosphate groups, are likely to form at lower pH than crimsonite. However, it should be noted that Keller (1977) reported that carminite formed at Tsumeb from solutions of relatively low pH. Pattersonite, the only one of these phases that contains an H_2O group, may form at a lower temperature, but in any case, it is almost as rare as crimsonite. Of course, in AsO_4-free environments, any of the above minerals would presumably be more likely to form than crimsonite.

Finally, it is worth noting that the octahedral site in crimsonite appears to strongly prefer Fe^{3+} over Al^{3+}. Evidence for this is seen in the other phosphates found in direct association with crimsonite, three of which contain essential Al and little or no Fe^{3+}: fluorwavellite, plumbogummite and variscite. Although plumbogummite has an Fe^{3+} analogue, kintoreite, the plumbogummite in association with crimsonite contains very little Fe^{3+}. Of the phosphates associated with crimsonite, only hentschelite contains essential Fe^{3+}.

The foregoing discussion provides some evidence that could be helpful in locating additional occurrences of crimsonite. In particular, we suggest that the mineral is most likely to occur in oxidized zones

of base-metal deposits in local environments that are rich in PO_4, but that contain a small amount of AsO_4. Clearly, Pb and Fe are necessary constituents in the system and Eh must be high enough that all (or most) of the Fe is present as Fe^{3+}. By analogy with carminite, the pH is likely to be relatively low. The most promising deposits to explore for crimsonite are those containing one or more of the aforementioned phases with essential Pb^{2+}, Fe^{3+} and PO_4^{3-}. Notably, in their description of kintoreite from the Kintore and Block 14 opencuts at Broken Hill, New South Wales, Australia, Pring et al. (1995) concluded that this mineral forms in the presence of solutions with high P/(As + S) ratios. They do not comment on the acidity of the solutions, but as noted above, kintoreite probably formed at relatively low pH, possibly lower than that required for the formation of crimsonite. We suggest that the PO_4-rich assemblages found in the Kintore and Block 14 opencuts at Broken Hill have a good potential for providing additional specimens of crimsonite.

Acknowledgements

References

Adams, P.A., Wise, W.S. and Kampf, A.R. (2015) The Silver Coin mine, Iron Point district, Humboldt County, Nevada. Mineralogical Record, **46**, 701–728.

Brese, N.E. and O'Keeffe, M. (1991) Bond-valence parameters for solids. Acta Crystallographica, **B47**, 192–197.

Brown, I.D. and Altermatt, D. (1985) Bond-valence parameters from a systematic analysis of the inorganic crystal structure database. Acta Crystallographica, **B41**, 244–247.

Chukanov, N.V., Pekov, I.V., Möckel, S., Zadov, A.E. and Dubinchuk, V.T. (2006) Zinclipscombite $ZnFe_2^{3+}$ $(PO_4)_2(OH)_2$ – a new mineral. Proceedings of the Russian Mineralogical Society, **135**, 13–18.

Gunter, M.E., Bandli, B.R., Bloss, F.D., Evans, S.H., Su, S.C. and Weaver, R. (2004) Results from a McCrone spindle stage short course, a new version of EXCALIBR, and how to build a spindle stage. The Microscope, **52**, 23–39.

Higashi, T. (2001) ABSCOR. Rigaku Corporation, Tokyo.

Kampf, A.R., Adams, P.M., Kolitsch, U. and Steele, I.M. (2009) Meurigite-Na, a new species, and the relationship between phosphofibrite and meurigite. American Mineralogist, **94**, 720–727.

Kampf, A.R., Adams, P.M., Housley, R.M. and Rossman, G.R. (2014) Fluorowardite, $NaAl_3(PO_4)_2F_2(OH)_2$ $(H_2O)_2$, the fluorine analogue of wardite from the Silver Coin mine, Valmy, Nevada. American Mineralogist, **98**, 804–810.

Kampf, A.R., Adams, P.M., Mills, S.J. and Nash, B.P. (2015a) Crimsonite, IMA 2014-095. CNMNC Newsletter No. 24, April 2015, page 249; Mineralogical Magazine, **79**, 247–251.

Kampf, A.R., Adams, P.M., Nash, B.P. and Marty, J. (2015b) Ferribushmakinite, $Pb_2Fe^{3+}(PO_4)(VO_4)(OH)$, the Fe^{3+} analogue of bushmakinite from the Silver Coin mine, Valmy, Nevada. Mineralogical Magazine, **79**, 661–669.

Kampf, A.R., Adams, P.M., Barwood, H. and Nash, B.P. (2015c) Fluorwavellite, IMA 2015-077. CNMNC Newsletter No. 28, December 2015, page 1862; Mineralogical Magazine, **79**, 1859–1864.

Keller, P. (1977) Paragenesis: Assemblages sequences, associations. Mineralogical Record, **8**, 38–47. [Special issue: Tsumeb! The world's greatest mineral locality (W.E. Wilson, editor)]

Kharisun, Taylor, M.R., Bevan, D.J.M. and Pring, A. (1996) The crystal structure of carminite: refinement and bond valence calculations. Mineralogical Magazine, **60**, 805–811.

Krivovichev, S.V. and Brown, I.D. (2001) Are the compressive effects of encapsulation an artifact of the bond valence parameters? Zeitschrift für Kristallographie, **216**, 245–247.

Mandarino, J.A. (1981) The Gladstone-Dale relationship: Part IV. The compatibility concept and its application. The Canadian Mineralogist, **19**, 441–450.

Mills, S.J., Kampf, A.R., Sejkora, J., Adams, P.M., Birch, W.D. and Plášil, J. (2011) Iangreyite: a new secondary phosphate mineral closely related to perhamite. Mineralogical Magazine, **75**, 329–338.

Mills, S.J., Sejkora, J., Kampf, A.R., Grey, I.E., Bastow, T.J., Ball, N.A., Adams, P.M., Raudsepp, M. and Cooper, M.A. (2012) Krásnoite, the fluorophosphate analogue of perhamite, from the Huber open pit, Czech Republic and the Silver Coin mine, Nevada. Mineralogical Magazine, **76**, 625–634.

Pouchou, J.-L. and Pichoir, F. (1991) Quantitative analysis of homogeneous or stratified microvolumes applying the model "PAP." Pp. 3l–75 in: Electron Probe Quantitation (K.F.J. Heinrich and D.E. Newbury, editors). Plenum Press, New York.

Pring, A., Birch, W.D., Dawe, J.R., Taylor, M.R., Deliens, M. and Walenta, K. (1995) Kintoreite, $PbFe_3(PO_4)_2(OH,H_2O)_6$, a new mineral of the

jarosite-alunite family, and lusungite discredited. *Mineralogical Magazine*, **59**, 143–148.

Roberts, A.C., Cooper, M.A., Hawthorne, F.C., Criddle, A. J. and Stirling, J.A.R. (2002) Sewardite, $CaFe_2^{3+}$ $(AsO_4)_2(OH)_2$, the Ca-analogue of carminite, from Tsumeb, Namibia: description and crystal structure. *The Canadian Mineralogist*, **40**, 1191–1198.

Sheldrick, G.M. (2008) A short history of SHELX. *Acta Crystallographica*, **A64**, 112–122.

Thomssen, D. and Wise, W.S. (2004) Special list: Silver Coin Mine, Iron Point district, Edna Mountains, Humboldt Co., Nevada, USA. *International Micromounter's Journal*, **13**, 7–8.